Heliyon 10 (2024) e40109

Contents lists available at ScienceDirect

Heliyon

journal homepage: www.cell.com/heliyon

Research article

Thermal wave and Pennes' models of bioheat transfer in human skin: A transient comparative analysis

Zerin Jahan Tasnim, R. Nasrin *

Department of Mathematics, Bangladesh University of Engineering and Technology, Dhaka, 1000, Bangladesh

ARTICLE INFO

Keywords:
TWMBT
Pennes' model
Human skin tissue
MW radiation
Relaxation time
FEM

ABSTRACT

The primary focus of this study is to analyze comparative heat transfer in a two-dimensional (2D) multilayered human skin using thermal waves and Pennes' bioheat transfer models. The model comprises the epidermis, dermis, hypodermis tissue, and inner cells, and aims to understand their response to microwave (MW) power and electromagnetic (EM) frequency. The system of equations involves EM wave frequency and bioheat equations and uses the finite element method (FEM) for solving. It encompasses a range of microwave power levels (4–16 W), frequencies (0.9–4 GHz), and exposure durations (0–180 s). It examines how MW power and frequency affect temperature predictions due to different relaxation times. The results are visually represented, illustrating microwave power dissipation, isothermal profiles within the skin tissue, temperature trends at several locations, relaxation times, specific absorption rate (SAR), and the mean surface temperature of the multilayered dermal cell. Thermal analysis shows that Pennes' equation predicts higher temperatures than the thermal wave model of bioheat transfer (TWMBT). A notable disparity in temperature evolution is observed between the two models, especially in high-frequency transient heating scenarios. The TWMBT forecasts a delay in heat transfer, offering valuable insights into the more realistic short-term thermal behavior that the classical Pennes' model fails to capture. This comparative study underscores the significance of selecting an appropriate bioheat transfer model for precise thermal analysis in biomedical applications, such as hyperthermia treatment and thermal diagnostics. The findings emphasize the potential of the TWMBT to enhance the accuracy of thermal treatments in clinical settings.

Nomenclature

Ai	Area of the different skin layers (m^2)
c	Specific heat of skin tissue (J/kg.°C)
c_b	Specific heat of blood (J/kg.°C)
C_t	Speed of the thermal wave (m/s)
$\mathbf{E}$	Electric field intensity (V/m)
f	Microwave frequency (Hz)
H	Height of the computational domain (m)
K	Thermal conductivity (W/(m.°C))
k	Wave number (m^{-1})
k_0	Wave number of free space (m^{-1})

(*continued on next page*)

* Corresponding author.
E-mail address: rehena@math.buet.ac.bd (R. Nasrin).

https://doi.org/10.1016/j.heliyon.2024.e40109
Received 18 April 2024; Received in revised form 15 October 2024; Accepted 1 November 2024
Available online 2 November 2024

(*continued*)

n	Normal vector
P	Input microwave power (W)
P_{abs}	Absorbed microwave power (W)
q_{mw}	Heat flux due to microwave power absorption (W/m^2)
Q_{met}	Metabolic heat source (W/m^3)
Q_{ext}	External heat source (W/m^3)
S	Effectiveness of the microwave absorption
SAR	Specific absorption rate (W/kg)
T	Actual temperature (°C)
T_b	Temperature of blood (°C)
T_m	Mean temperature (°C)
t	Time (s)
W	Width of computational domain (m)
z	Penetration depth (m)
Greek Symbols	
α_0	Thermal diffusivity ($m^2\ s^{-1}$)
$\alpha(f)$	Frequency-dependent attenuation coefficient
ε_0	Permittivity of free space (F/m)
ε_r	Relative permittivity
μ	Permeability (H/m)
μ_r	Relative permeability
λ	Wave length (m)
η	Absorption efficiency
ρ_b	Density of blood (kg/m^3)
σ	Electric conductivity of tissue (S/m)
τ	Relaxation time (s)
ω	Angular frequency (rad/s)
ω_b	Blood perfusion rate (1/s)

1. Introduction

The human skin has four layers: the epidermis, dermis, hypodermis, and underlying cells. Microwave radiation can affect biological tissues, causing thermal and physiological effects. Bioheat transfer examines thermal energy exchange in biological tissues, including heat generation, absorption, transmission, radiation, and conduction.

Understanding the interaction between microwave energy and biological tissues, particularly in the context of skin, is crucial for various fields. Accurate monitoring and analysis are necessary to ensure safety and effectiveness [1]. Researchers use measurable data to understand how EM energy is absorbed by the human body when directly exposed to intense radiation [2–4].

The effects of absorbing EM energy depend on factors like intensity, waveform, frequency, and duration of exposure [5]. Millimeter waves (mmWs) are primarily absorbed by the skin, leading to localized temperature changes [6]. The absorption of electromagnetic energy by biological tissue leads to ion acceleration and molecular collisions, raising the local tissue temperature. Even a slight increase in body temperature (1–5 °C) can have adverse effects, including deformities, brain lesions, temporary male infertility, and changes in blood chemistry [7].

Prior studies have reported on the effects of radiofrequency (RF) and microwave radiation on human body temperature. Peyman et al. [8] studied the impact of RF radiation on SAR values in children. Wessapan et al. [9] used bio-thermal equations to investigate temperature increases in the brain, eyes, and human trunk caused by RF waves. Kojima and colleagues [10] studied the effects of thermal changes caused by millimeter waves on the eyes. In 2006, Stewart and associates [11] examined skin heating from prolonged exposure to 94 GHz. Mukeddes et al. [12] observed the intensity of burns from heat exposure on human skin. The threshold values for incident power density have been authoritatively established by Lin and Wang [13], as well as confirmed by Ziskin and Morrissey [14]. The foundational framework for understanding heat transfer within human tissue was formulated by Pennes in 1948 through the bioheat equation (BHE). Researchers have adapted Pennes' model to create mathematical bioheat models for specific scenarios. Tissue damage becomes irreversible at 40–45 °C temperatures after prolonged exposure [15].

In their 2017 study, Lin and Li [16] analyzed heat conduction in the three-layer structure of human skin using a semi-analytical approach. They investigated the effects of different parameters on temperature fluctuations and thermal damage potential. Amare et al. [17] conducted human body heating experiments using a sophisticated replication infrastructure. Gurung and Shrestha [18] studied abnormal thermal regulation in human skin, highlighting temperature changes due to sweating and ambient fluctuations. Dutta et al. [19] provided an exact analysis of bio-heat transfer models, including classical, single-phase-lag, and dual-phase-lag, for a single layer of living tissue. This analysis enabled precise predictions of thermal responses, which can assist in optimizing treatment protocols for thermal therapies. Keangin and colleagues [20] conducted numerical simulations of liver cancer treatment, considering heat transfer, electromagnetic wave propagation, and mechanical deformation in biological tissues. The research also covered a variety of antenna types and the effects induced by porous media [21,22].

Biswas et al. [23] studied microwave ablation for liver cancer therapy, focusing on temperature, MW power, and SAR distribution assessments. Expanding upon these foundations, a more expansive TWMBT was introduced by Tung et al. [24], Fazlali et al. [25], Dutta and Kundu [26], and Marin et al. [27]. Their contributions sought to enhance the understanding of bioheat transfer in living tissues, a domain marked by its intricate nature. The intricacies of diverse biological environments, such as the human body,

emphasize the importance of relaxation time in influencing the speed of electromagnetic wave response to heat conduction in biological tissue [28].

The thermal relaxation time for meat products is approximately 20–30 s [29,30]. Biological materials have longer relaxation times compared to conventional materials. Rapid heating processes like burn injuries, scald treatments, freeze injuries, laser radiation, and traditional cancer hyperthermia procedures show distinct thermal wave properties.

The complexities of thermal wave effects in bioheat transfer are not well understood. Traditional modeling approaches like Pennes' equation are inadequate. To fill this gap, Liu and colleagues [31] used the separation of variables method to study one-dimensional thermal wave bioheat transfer in a finite medium. Dutta et al. [32] and Kundu [33] applied the separation of variables method to derive the exact temperature response in biological tissue for both Fourier and non-Fourier heat conduction models, specifically in therapeutic applications. However, there is limited research on the effects of relaxation times on heat transfer in the cranial region. To our knowledge, Kaur and Khan [34] are the only researchers able to estimate thermal alterations in the human head when exposed to MW radiation. Kaur studied the effect of relaxation times on abdominal temperature variations from 2450 MHz MW exposure at different power levels. Subsequent studies have demonstrated that higher relaxation times correspond to lower predicted temperatures [35–42].

Based on the evaluation above, it becomes evident that numerous researchers have focused on studying thermal transport in dermal cells confronted with MW through utilizing TWMBT. However, according to the author's insights, certain areas warrant further investigation, including.

- Although thermal transport in human skin tissues exposed to microwave radiation using TWMBT has profound implications, research has been scarce in this domain.
- This field offers considerable opportunities to predict temperature distribution inside different layers of the human skin.
- The investigation of strategies for managing the escalating unsteady temperatures associated with varying microwave input power and frequency has remained relatively unexplored.

This analysis's fundamental objective is to give researchers profound insights into the judicious employment of plane microwave exposure. This encompasses the meticulous consideration of pivotal factors, including carefully selecting the most suitable MW frequency, the precise determination of input power levels, and the astute incorporation of relaxation time. The anticipated outcomes arising from the diligent pursuit of this study are poised to function as a wellspring of inspiration for both the readership and fellow researchers, effectively catalyzing a deeper foray into the intricate domain of thermal analysis concerning dermal cells during MW radiation, with a specialized focus on the TWMBT.

We take the initiative to explore the following.

- It offers a comprehensive comparative analysis of how two-dimensional multilayered skin tissue responds thermally to MW exposure of TWMBT and Pennes' models.
- The impact of various factors such as MW input power, frequency, and relaxation time on microwave power dissipation density and the isothermal line absorbed by skin tissue is investigated.
- The intricate dynamics involving bioheat transfer, the temperature field, and the progression of EM waves within the context of genial dermatological cells when they endured direct exposure to intense MW radiation is observed.
- The spatial distribution of SAR throughout the entire dermal tissue, along with the average temperature and surface temperature distribution, is encompassed.

In essence, this numerical investigation is designed to establish itself as an enduring foundational reference, one that is strategically

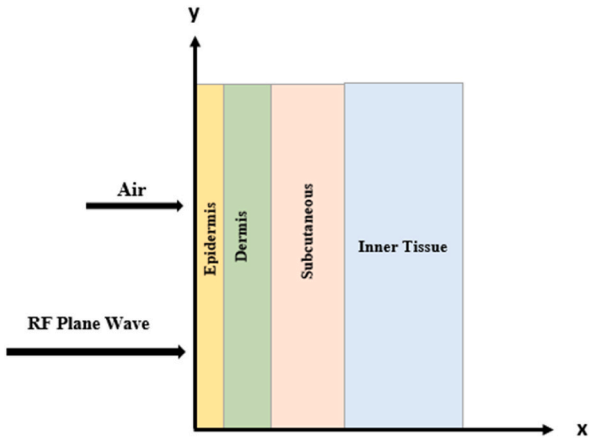

Fig. 1. Four-layered human skin model.

poised to provide invaluable guidance and insights for medical practitioners. It is an indispensable resource for those within the medical community who harbor a genuine interest in broadening their understanding of clinical thermal technology and the various facets of thermal medical practices. This sets our research apart from previous research.

2. Physical model

This model, characterized by intricacy, encompassed four distinct layers: the outermost superficial layer, underlying dermis, hypodermis, and subjacent cells that served as representations of the body's core. The propagation of electromagnetic fields emanating from an EM radiation device towards the human self is visually portrayed in Fig. 1. A uniform distribution of incident irradiance per unit area across the entire exposure area is assumed for the sake of the analysis. Comprehensive breakdowns of the dielectric properties of the dermal layers at diverse frequencies and the corresponding thermal properties associated with these layers are provided in Tables 1 and 2 in our documentation. In the direction of the x-axis, the transverse magnetic (TM) plane MW is applied to the human body's skin model. The computational domain has width, W (=0.03 m) and height, H (=0.02 m). The FEM is utilized in our mathematical inquiry, and a virtualization software governed by a couple of partial differential equations (PDEs) is employed for computational procedure.

3. Governing equations

Adopting a 2D model like the TWMBT provides several benefits when studying temperature distribution within human skin. It offers better spatial resolution, accommodates complex boundary conditions, improves accuracy in temperature predictions, and allows for more precise visualization and interpretation of results. This model employs the bioheat transfer interface and the electromagnetic frequency domain interface for transient analysis.

3.1. Electromagnetic wave frequency model

To streamline the complexity of this research, we have embraced the following assumptions.

- ❖ The interaction between human skin and microwaves occurs in an unobstructed environment, meaning the skin model lacks surrounding walls or metallic enclosures.
- ❖ Scattering boundary conditions are applied to confine the electromagnetic fields in free space.
- ❖ The microwaves are considered plane waves, specifically in the TM mode, traveling in the positive x-axis direction.
- ❖ Uniform and consistent dielectric properties are assumed across all tissue layers.

Electromagnetic wave propagation within human skin involves the utilization of Maxwell's equation (1) according to Ref. [34].

$$\nabla \times \frac{1}{\mu_r}(\nabla \times \mathbf{E}(x,y,t)) - k_0^2\left(\varepsilon_r - \frac{j\sigma}{\omega\varepsilon_0}\right)\mathbf{E}(x,y,t) = \mathbf{0}, \tag{1}$$

where, electric field intensity $\mathbf{E}$ (V/m), relative magnetic permeability μ_r, relative permittivity ε_r, permittivity of free space $\varepsilon_0 = 8.8542 \times 10^{-12}$ (F/m), imaginary unit $j = \sqrt{-1}$, wave number in free space k_0 (m^{-1}), biological tissue conductivity σ, and angular frequency ω (rad/s).

For this research, the boundary and the initial conditions are considered to be the same for both the physics of EM wave frequency and bioheat transfer.

3.1.1. Boundary and initial conditions for wave propagation [23,34]

Intrinsic scattering boundary conditions proficiently avert the advent of undesired reflective phenomena. At the outer edges of the computational domain (Fig. 2) it is equation (2):

$$\left.\begin{array}{c}\mathbf{n} \times (\nabla \times \mathbf{E}(x,y,t)) - jk\mathbf{n} \times (\mathbf{E}(x,y,t) \times \mathbf{n}) = \mathbf{0} \\ \text{or}, -\mathbf{n} \times (\mathbf{E_0}(x,y,t) \times jk(\mathbf{n} - k))exp(-j\mathbf{k} \bullet \mathbf{r}(x,y)) = \mathbf{0}\end{array}\right\}. \tag{2}$$

where, k, $\mathbf{E_0}(x, y, t)$ and $\mathbf{n}$ assume wave number (m^{-1}), incident plane wave (V/m) and normal vector, respectively.

Wave port boundary condition governs the incident plane microwaves in the TM mode as they impinge upon this region of the

Table 1
Thermos-physical characteristics of several dermal structures [1].

Layer	Specific heat c_p	Thermal conductivity k	Mass density ρ	Blood perfusion rate ω_b	Thickness x (m)
Epidermis	3578–3600	0.21–0.26	1200	0	7.0E-4
Dermis	3200–3400	0.36–0.52	1200	1.5	0.0012
Subcutaneous	2288–3060	0.16–0.21	1200	1.5	0.008
Inner tissue	4000	0.5	1200	1.5	0.02

Table 2
The electro-insulative characteristics of the stratified dermal structures across diverse frequency domains [5,9,34].

Layer	$f = 0.9$ GHz		$f = 1.8$ GHz		$f = 2.45$ GHz		$f = 4$ GHz	
	ε_r	σ	ε_r	σ	ε_r	σ	ε_r	σ
Epidermis	3.02	0.011	4.08	0.12	4.01	0.010	3.07	0.111
Dermis	5.12	0.242	5.11	0.66	5.00	0.383	4.68	0.498
Subcutaneous	4.81	0.033	4.20	0.32	4.68	0.091	3.98	0.130
Inner tissue	27.85	0.345	24.70	0.98	24.32	0.965	25.40	1.415

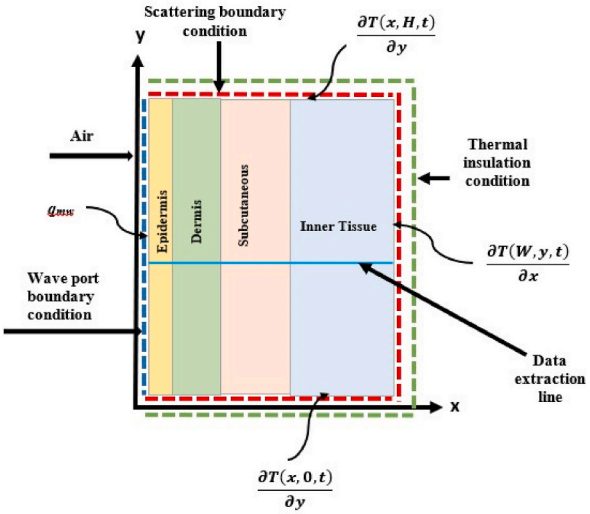

Fig. 2. Boundary conditions.

dermal cell (equation (3)).

$$S = \frac{\iint((\mathbf{E}(x,y,t) - \mathbf{E_1}(x,y,t)).\mathbf{E_1}(x,y,t))dA_i}{\iint(\mathbf{E_1}(x,y,t).\mathbf{E_1}(x,y,t))dA_i}. \tag{3}$$

Where S represents a measure of the effectiveness of the MW absorption, $\mathbf{E_1}(x,y,t)$ designates the wave port's fundamental electric field (V/m), A_i is the area (m^2) of the epidermis layer ($i = 1$).

3.2. Bioheat transfer model

To mitigate the intricacy inherent in the research, we introduce the subsequent assumptions.

- ❖ Cutaneous cells are biomaterials characterized by unalterable thermal properties attributes.
- ❖ There are no alterations in the phase of substances.
- ❖ Localized thermal equilibrium between the circulatory blood and the adjacent tissue.
- ❖ The absence of chemical reactions is a prevailing characteristic within the confines of the cutaneous cell.

Two pertinent thermal models are harnessed to scrutinize and elucidate tissue behavior concerning the intricate dynamics of heat transfer when confronted with exposure to MW radiation. The Pennes' bioheat transfer model, which incorporates perfusion and metabolic heat generation, is compared with the thermal wave model that considers finite thermal propagation speed, introducing a hyperbolic nature to the heat conduction equation.

3.2.1. Model I: Pennes' bioheat equation (BHE) [45,46]

Pennes' bioheat equation proves to be a highly effective approach for characterizing the heat transfer mechanisms within the tissue in equation (4):

$$\rho c \frac{\partial T(x,y,t)}{\partial t} = \nabla.(K\nabla T(x,y,t)) + \rho_b c_b \omega_b (T_b - T(x,y,t)) + Q_m(x,y,t) + \quad Q_{ext}(x,y,t). \tag{4}$$

where, density ρ (k g/m^3), specific heat at constant pressure c (J/kg.K), thermal conductivity K (W/m·K), blood density ρ_b (k g/ m^3),

blood specific heat c_b (J/kg·K), the tissue temperature at any point and blood temperature $T(x, y, t)$ and T_b (°C), respectively, blood perfusion rate ω_b (1/s), power density induced by metabolic process, and external heat source $Q_m(x,y,t)$ and $Q_{ext}(x,y,t)$ (W/ m^3), respectively.

The expression $\nabla.(K\nabla T(x,y,t))$ of equation (4) encapsulates the fundamental concept of heat conduction operative within the skin tissue, drawing its theoretical foundation from Fourier's law (equation (5)):

$$\mathbf{q}(x,y,t) = -K\nabla T(x,y,t). \tag{5}$$

Blood perfusion is a mechanism to estimate and approximate the heat conduction between the tissue and the blood flow, expressed by:

$$\rho_b c_b \omega_b (T_b - T(x,y,t)).$$

3.2.2. Model II: thermal wave model of bioheat transfer (TWMBT)

The pioneering concept of thermal lag is meticulously interwoven into the core of Fourier's law by deliberately introducing a relaxation time parameter unequivocally denoted as 'τ'. This innovative development is elegantly presented and outlined in equation (5), exemplified as follows (equation (6)):

$$\mathbf{q}(x,y,t+\tau) = -K\nabla T(x,y,t). \tag{6}$$

We can derive a novel TWMBT, where $\tau = \alpha/C_t^2$, with α and C_t denoting the thermal diffusivity (m^2/s) and speed of the thermal wave in the medium (m/s).

$$\begin{aligned}\rho c\tau\frac{\partial^2 T(x,y,t)}{\partial t^2} = {} & K\nabla^2 T(x,y,t) - \rho_b\, c_b\, \omega_b\, T(x,y,t) - (\tau\rho_b\, c_b\, \omega_b + \rho c)\frac{\partial T(x,y,t)}{\partial t} + \rho_b\, c_b\, \omega_b T_b(x,y,t) + Q_{met}(x,y,t) \\ & + Q_{ext}(x,y,t) + \tau\frac{\partial Q_{met}(x,y,t)}{\partial t} + \tau\frac{\partial Q_{ext}(x,y,t)}{\partial t}.\end{aligned} \tag{7}$$

Where, $\nabla = \left(\mathbf{i}\frac{\partial}{\partial x} + \mathbf{j}\frac{\partial}{\partial y}\right)$, and $\nabla^2 = \left(\frac{\partial^2}{\partial x^2}, \frac{\partial^2}{\partial y^2}\right)$.

Since Q_{met} is assumed zero in our analysis, equation (7) can be re-written as:

$$\rho c\tau\frac{\partial^2 T(x,y,t)}{\partial t^2} = K\nabla^2 T(x,y,t) - \rho_b\, c_b\, \omega_b\, T(x,y,t) - (\tau\rho_b\, c_b\, \omega_b + \rho c)\frac{\partial T(x,y,t)}{\partial t} + \rho_b\, c_b\, \omega_b T_b(x,y,t) + Q_{ext}(x,y,t) + \tau\frac{\partial Q_{ext}(x,y,t)}{\partial t}. \tag{8}$$

It is paramount to emphasize that when the τ assumes a null value, denoted as $\tau = 0$, within the construct of equation (8), it undergoes a remarkable metamorphosis, effectively reverting to the original state as represented by equation (4).

3.2.3. Boundary and initial conditions for bioheat transfer [23,32,34,43]

The boundary conditions are explicitly defined as follows (equations (9)–(12)):

$$\text{At } x = 0, -k\frac{\partial T(0,y,t)}{\partial x} = q_{mw}\,. \tag{9}$$

$$\text{At } x = W, \frac{\partial T(W,y,t)}{\partial x} = 0\,. \tag{10}$$

$$\text{At } y = 0, \frac{\partial T(x,0,t)}{\partial y} = 0\,. \tag{11}$$

$$\text{At } y = H, \frac{\partial T(x,H,t)}{\partial y} = 0. \tag{12}$$

The heat flux due to MW (or mw) power absorption of equation (9) is

$$q_{mw} = \eta\frac{P_{abs}}{A_i}, \tag{9a}$$

and the absorbed MW power (P_{abs}) is related to frequency (f) and power (P) such as

$$P_{abs}[W] = P\left(1 - e^{-2\alpha(f)z}\right), \tag{9b}$$

Thus, the boundary condition of (9) can be written as:

$$-k\frac{\partial T(0,y,t)}{\partial x} = \eta\frac{P\left(1 - e^{-2\alpha(f)z}\right)}{A_i} \tag{9c}$$

where, z is the penetration depth (m) of the MW into the tissue, $\alpha(f)$ is the frequency-dependent attenuation coefficient, η is the absorption efficiency of the MW energy, Ai is the area (m^2) of the epidermis layer ($i = 1$) over which the MW is applied.

The mean temperature of the skin tissue layer domain can be evaluated using equation (13) as Biswas et al. [23]:

$$T_m(t) = \frac{\iint T\, dA_i}{\iint dA_i}, \tag{13}$$

where A_i is the area (m^2) of the different skin layers and $i = 1, 2, 3, 4, 5$ represents the epidermis, dermis, subcutaneous, inner layer, and total computational domain, respectively.

Fig. 2 represents the total boundary conditions of this model at a glance.

3.3. Interaction of human tissues and EM fields [23]

The heat generated by the dissipation of an electromagnetic wave in tissue is referred to as the equations' (4, 8) external heat source (Q_{ext}). In microwave heating, the applied heat load function (Q_{ext}) represents the power absorbed per unit volume of tissue due to microwave exposure. The absorbed EM heat source density Q_{ext} (W/m^3) is formally defined as follows (equation (14)):

$$Q_{ext}(x, y, t) = \frac{1}{2}\sigma(\mathbf{E}(x, y, t) \bullet \mathbf{E}(x, y, t)), \tag{14}$$

where σ is electrical conductivity (S/m).

When EM waves propagate through the tissue, the tissue absorbs the energy of the waves. When determining the electric field value at a point within skin tissue, the heat generated from MW-associated EM energy is calculated using equation (14).

The microwave frequency and power influence the magnitude and distribution of this heat load function. The SAR constitutes a metric designed to assess and quantify the mean power absorption per unit of mass in cellular material (equation (15)).

$$\mathrm{SAR} = \frac{\sigma(\mathbf{E}(x, y, t) \bullet \mathbf{E}(x, y, t))}{2\rho}\ (\mathrm{W/kg}). \tag{15}$$

4. Solution procedure

The FEM is employed in conjunction with Galerkin's method of weighted residual [47]. The primary objective is the solution of a 2D numerical model of a BHE, which involves a system of intricate PDEs (1, 4–5). The comprehensive system of governing equations, encompassing time-dependent BHE and EM wave frequency considerations, is expertly solved, diligently considering the specified initial and boundary conditions. The endeavors culminated in acquiring an unsteady solution, effectively spanning the temporal range (0–180 s), providing a detailed representation of the evolving temperature field over the specified time interval.

In the methodology adopted, the expansive solution domain is subjected to meticulous discretization, resulting in its thorough partition into finite element meshes, primarily characterized by the strategic inclusion of non-uniform triangular elements across various domains and boundaries. Subsequently, equation (1) and (4–5) underwent a systematic transformation, leading to their evolution into a comprehensive system of integral equations. The paramount variables encompassed by these governing equations included the electric field ($\mathbf{E}$) and temperature (T). The Gauss quadrature method and exact integration formulas are meticulously and thoughtfully employed to ensure the precision of numerical integration for every constituent term.

The resulting algebraic equations are adjusted to account for boundary conditions. We employ six-node triangular elements, each associated with the electric field and temperature, to maintain consistency with our numerical research. The resolution of this

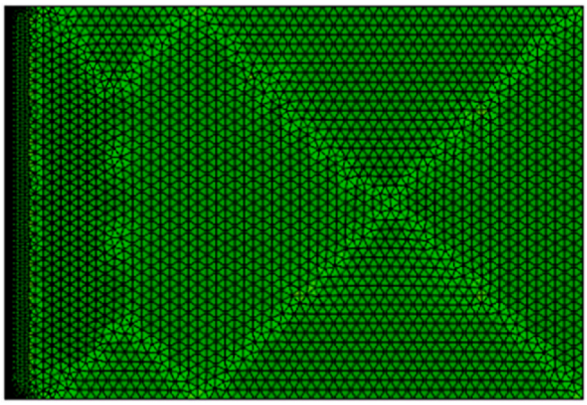

Fig. 3. Mesh generation of the computational domain.

comprehensive set of linear algebraic equations is determined using the Newton-Raphson iteration technique. Following this transformation, the linear algebraic equations are addressed using a triangular factorization method. The convergence criterion for the solution procedure is precisely defined as $|\psi^{i+1} - \psi^{i}| \leq 10^{-4}$, where '$i$' represents the number of iterations, and 'ψ' is a function that depends on both **E** and T [43,44].

4.1. Mesh generation

The strategy for mesh generation is defined by non-uniform triangular elements, with each component comprising six nodes distributed across the domain. Separate mesh generations are made to consider four layers to calculate thermal response. Fig. 3 illustrates the generation of the finite element mesh in an 'extra fine' configuration. In this meshing setup, the computational region encompasses numerous vertex and edge elements, ensuring a minimum element quality. The aggregate count of elements is 47,976, consisting of 5041 for vertex elements and 5890 for edge elements, each representing their respective element quality. Specific element sizes are stipulated in this particular mesh configuration, with a maximum length of 6.0E-4 m and a minimum of 2.25E-6 m. Furthermore, the curvature mesh resolution is established at 0.25, while the resolution for narrower regions is designated 1. The upper limit for element growth rate has been restricted to 1.2.

4.2. Grid-independent test

To perform a comprehensive grid sensitivity analysis, we examine five distinct mesh configurations, with each configuration being delineated by the subsequent parameters: frequency (f) 2.45 GHz, power (P) 12 W, relaxation time (τ) 20 s, and time (t) 180 s. Corresponding grid concentrations are 20,463 degrees of freedom, 2072 elements; 22,546 degrees of freedom, 2277 elements; 29,507 degrees of freedom, 2938 elements; 58,907 degrees of freedom, 5890 elements; and 1,82,970 degrees of freedom, 18257 elements. The optimum value of the SAR is assumed to be the supervising parameter for checking the correctness of the numerical solution. Considering values of obtained SAR, the current simulation is conducted with grid management of 58,907 degrees of freedom and 5892 elements. Table 3 shows that any additional development in precision does not occur with a superior number of degrees of freedom and finite elements.

4.3. Coding validation

The study validates the temperature versus time results obtained from the current code by comparing them with those of Torvy and Dale [48], as shown in Fig. 4. The comparison illustrates the temperature-time histories for the basal layer of human skin exposed to a flash fire with a heat flux of 4186 W/m^2 for the initial 10 s and 0 W/m^2 from 11 to 60 s, serving as a benchmark. The researchers utilized Pennes' bioheat transfer model as the governing equation and employed the finite element method (FEM) to solve the model. The data is extracted from their research using GetData Graph Digitizer software. In this code validation, the x-axis represents time (0–60 s) and the y-axis represents temperature (35–55 °C). Both datasets exhibit a similar pattern: initially, the temperature rises to around 52 °C at 30 s, followed by a decrease. The maximum error value is measured as 1.74 % for this coding validation. The agreement between the current code result and Torvy and Dale's [48] results is excellent. This agreement demonstrates the reliability of our coding and boosts our confidence in applying it for further research.

5. Results and discussions

The human skin model meticulously implemented within our simulation framework comprised a carefully delineated architecture, encompassing four distinct strata: the depth of the air domain is 1.0E-5 m; epidermis characterized by a depth of 7.0E-4 m; the dermis, extending to a depth of 0.0012 m; the hypodermis layer, which possessed a thickness of 0.008 m; and the subjacent cells, spanning to a depth of 0.02 m. This intricate model adhered to specific spatial dimensions, measuring 0.03 m along the x-axis and 0.02 m along the y-axis, ensuring a precise and accurate representation of the complex anatomical structure under scrutiny. We explore the effects of microwave frequency (f), input power (P), and relaxation time (τ) over a wide range of values, spanning 0.9–4 GHz, 4–16 W, and 0–40 s, respectively. The numerical simulation covers a time range from 0 to 180 s. This investigation emphasizes a specific and intentional focus on thoroughly examining the thermal dynamics associated with skin exposure to MW radiation.

5.1. Effect of EM frequency

Figs. 5–9 elucidate the intricate dynamics whereby MW frequencies spanning the spectral expanse from 0.9 to 4 GHz exert

Table 3
Grid test with $f = 2.45$ GHz, $P = 12$ W, $\tau = 20$ s, and $t = 180$ s.

Mesh type	Normal	Fine	Finer	Extra Fine	Extremely Fine
Degrees of freedom	20463	22546	29507	58907	182970
Elements	2072	2277	2938	5890	18257
SAR (W/Kg)	357.5132	357.8341	358.0154	358.1013	358.1014

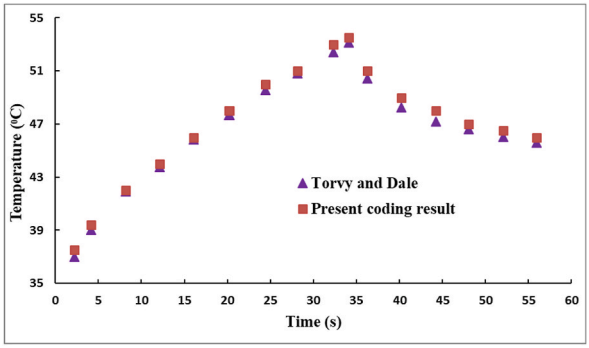

Fig. 4. Temperature versus time scenario between the results of (Torvy and Dale [48]) and present code.

discernible influence upon an array of parameters intricately linked to the phenomenon of MW absorption within the complex milieu of human dermal tissue using TWMBT. In these simulations, a relentless adherence to unvarying values is observed concerning supplementary parameters, wherein the magnitude of power remains fixed at $P = 12$ W, and the duration of exposure remains in unwavering stasis at $\tau = 20$ s.

Within the confines of Fig. 5 (i-iv), we discern a meticulously portrayed representation of the microwave power density undergoing absorption by the dermal tissue layer at a specific temporal juncture denoted by $t = 50$ s, in the context of four discrete microwave frequencies, namely, 0.9 GHz, 1.8 GHz, 2.45 GHz, and 4 GHz. The graphical representation in question elucidates that microwave absorption is highest near the region where the incident waves are nearly plane. Additionally, the differences between absorption

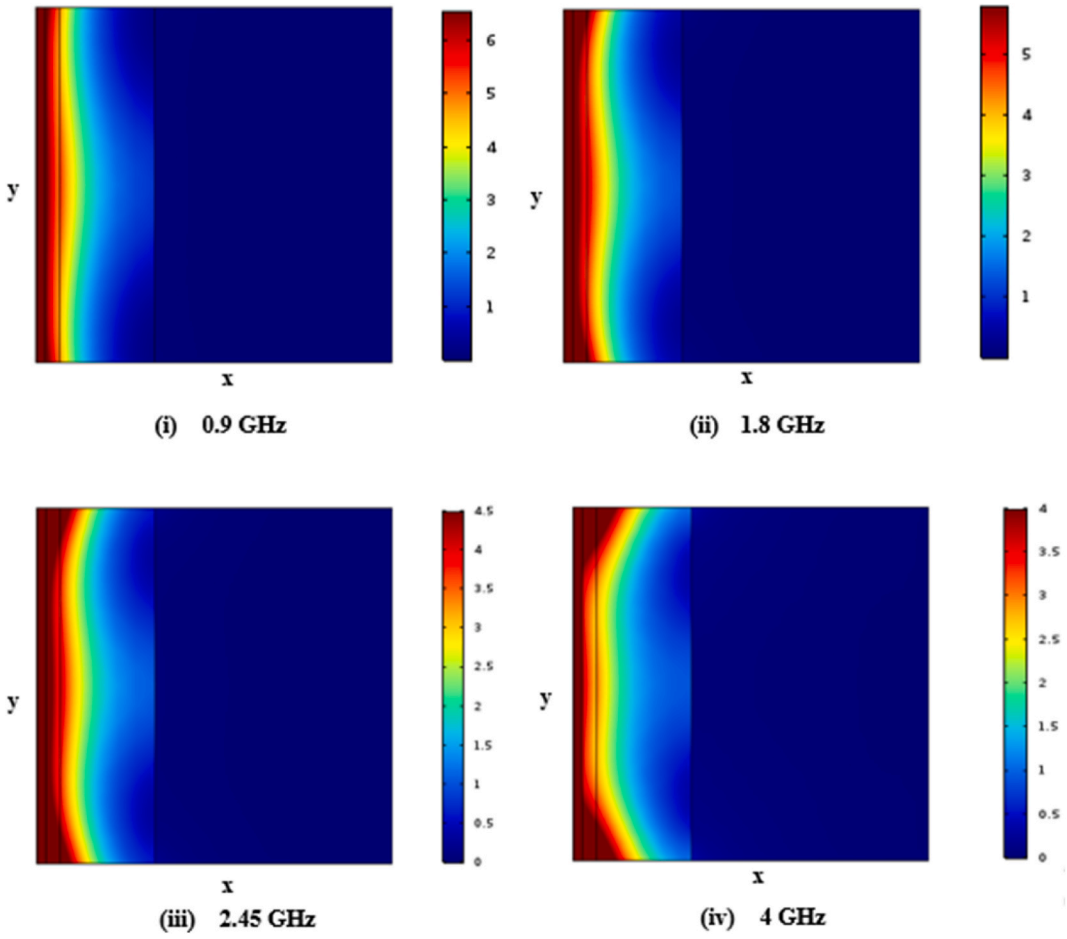

Fig. 5. Impact of MW frequencies (*f*), (i) 0.9 GHz, (ii) 1.8 GHz, (iii) 2.45 GHz, and (iv) 4 GHz, on MW power dissipation density absorbed by skin, with $P = 12$ W, $\tau = 20$ s, and $t = 50$ s.

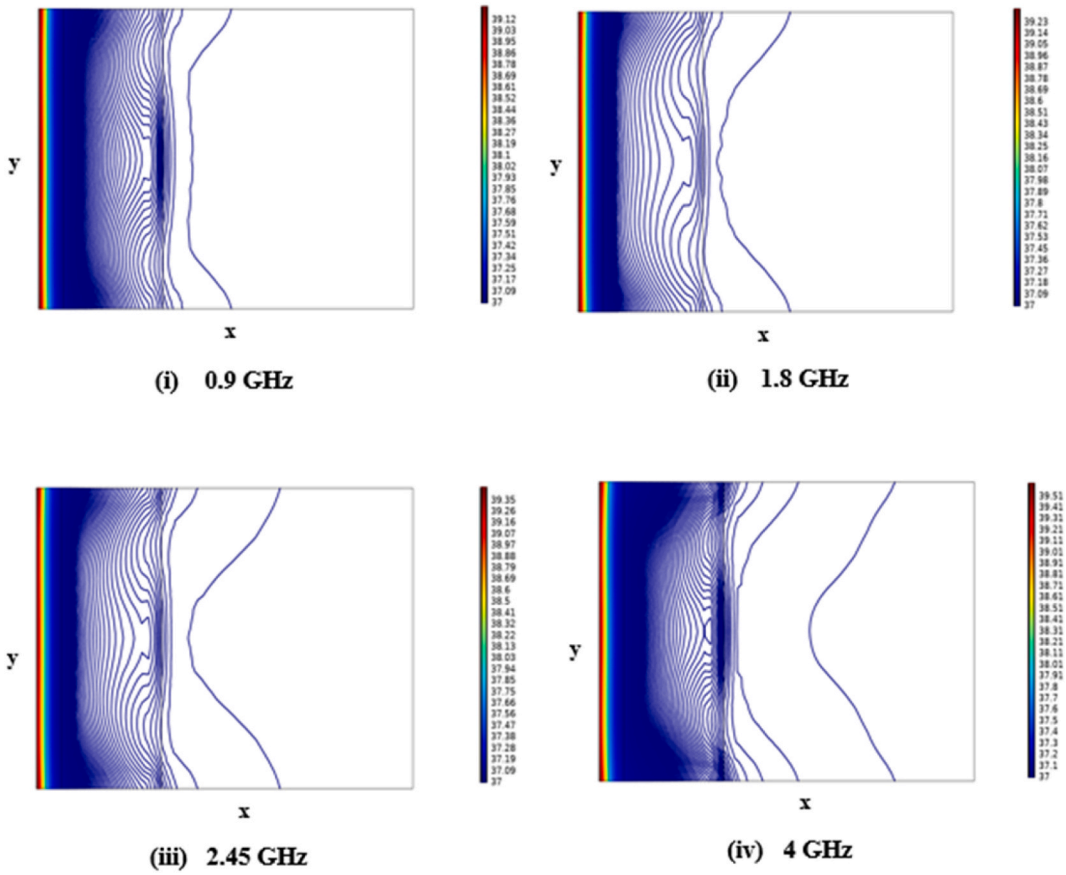

Fig. 6. Impact of MW frequencies (f), (i) 0.9 GHz, (ii) 1.8 GHz, (iii) 2.45 GHz, and (iv) 4 GHz, on isothermal lines with $P = 12$ W, $\tau = 20$ s, and $t = 50$ s.

levels for the four tested frequencies diminish as frequency increases. Notably, when the frequency reaches 4 GHz, the heated area becomes small and is not uniformly heated simultaneously. As the frequency continues to increase, the entire skin layer experiences heating. In close adjacency to the vicinity of exposure, characterized by the vehement concentration of the heat source, one discerns the manifestation of elevated thermal states. In contrast, at a greater remove from the immediate reach of the incident waves, wherein the influence of the heat source decreases, the physiological circulatory system of the organism adeptly manages to uphold the tissue's temperature at the standard equilibrium of the human body. The derived computational assessment of microwave heat source density evinces its most elevated magnitudes near the designated exposure zone.

Fig. 6 (i-iv) shows thermal distribution contour lines in biological tissue at a specific time ($t = 50$ s) for four distinct microwave frequency values. These contour lines are consistent and illustrate the computed ellipsoidal shapes. Within the scope of our analytical investigation, we embarked upon our scholarly endeavor by establishing an initial skin temperature quantified at 37.15^0 C. Precisely, at the discrete microwave frequencies of 0.9 GHz, 1.8 GHz, 2.45 GHz, and 4 GHz, our observations unveil the attainment of maximal temperature increments, which manifest as 39.12 °C, 39.23 °C, 39.35 °C, 39.52 °C, respectively. Interestingly, we notice that the temperature significantly rises within the exposure area but rapidly decreases as we move away from it. Overall, the skin's temperature profile remains within an acceptable range. Predicated upon the discerned outcomes derived from our investigations, we deduce that the ramifications of exposure to mmWs upon the thermal equilibrium of skin tissue are, in practical terms, characterized by a marginal and inconsequential influence, signifying a negligible perturbation in skin temperature. Therefore, the likelihood of thermal hazards arising from MW frequency exposure is minimal.

Within Fig. 7 (i-iv), we expound upon the temporal evolution of mean temperature (T_m) across distinct layers of skin using equation (13), encompassing the epidermis, dermis, subcutaneous, and inner tissue layers, specifically scrutinized at a designated temporal juncture ($t = 180$ s), while subjected to an array of diverse MW frequencies. The behavior of these mean temperature curves varies depending on the MW frequency. For lower MW frequencies, the curves primarily reflect the influence of the radiation source, resulting in a linear mean temperature increase. Nevertheless, as the mean temperature progressively converges toward a particular critical threshold, the intricate interplay of variables, including diffusion mechanisms and the conveyance of heat through the conduit of blood perfusion, begin to exert their influence, culminating in the phenomenon of MW absorption.

In the epidermis layer, we observe maximum mean temperature (T_m) of 38.39 °C for a MW frequency of 0.9 GHz, 38.98 °C for 1.8

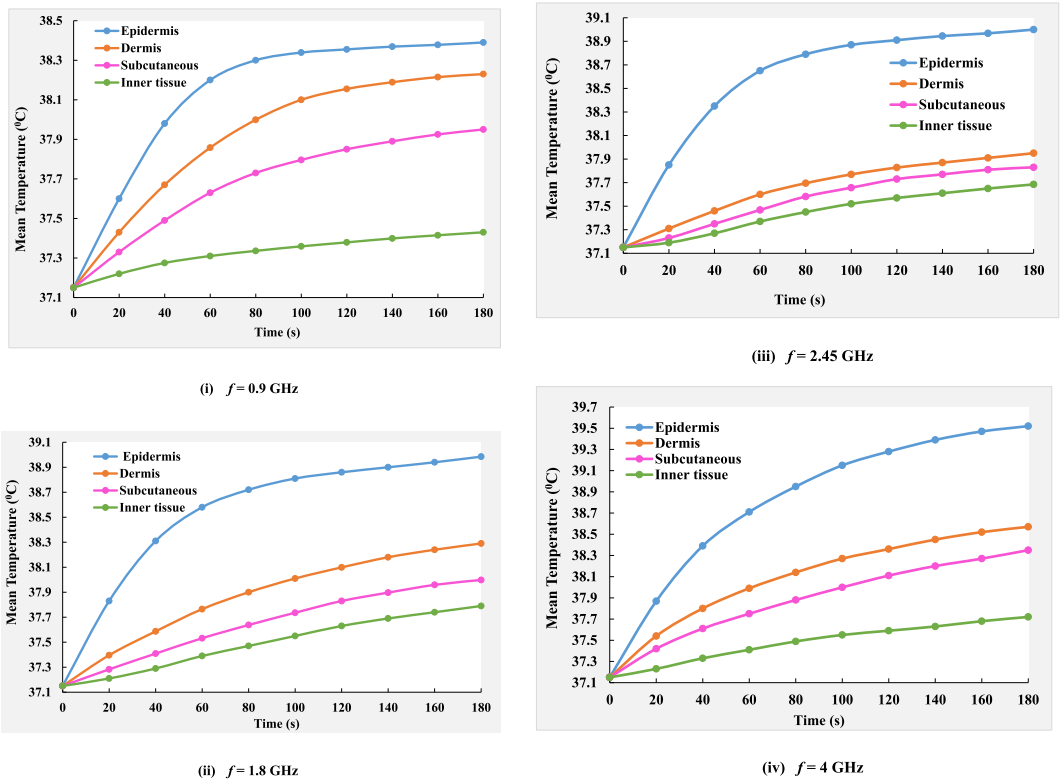

Fig. 7. Impact of MW frequencies (f), (i) 0.9 GHz, (ii) 1.8 GHz, (iii) 2.45 GHz, and (iv) 4 GHz on the mean temperature (T_m) of different layers at different time with $P = 12$ W, $\tau = 20$ s.

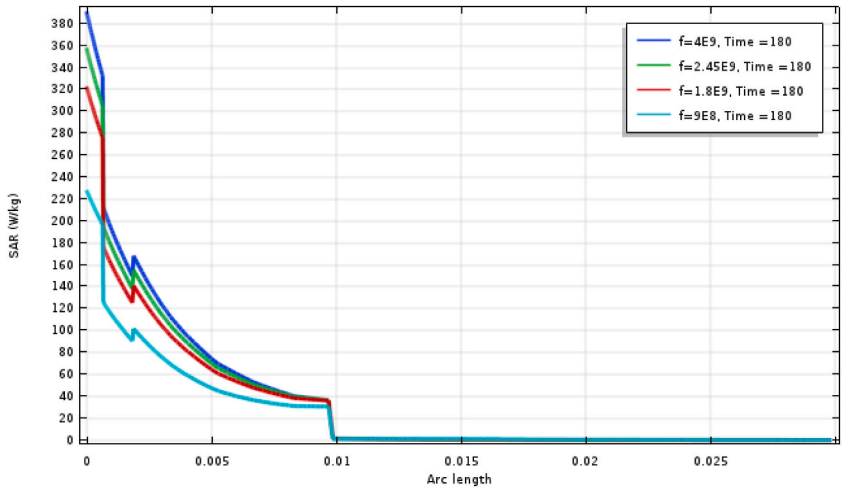

Fig. 8. The axial profile of SAR due to MW frequencies (f), (i) 0.9 GHz, (ii) 1.8 GHz, (iii) 2.45 GHz, and (iv) 4 GHz with $P = 12$ W, $\tau = 20$ s, and $t = 180$ s.

GHz, 39.00 °C for 2.45 GHz, and 39.52 °C for 4 GHz, all at $t = 180$ s. The upper limit of T_m augmentation discerned within the epidermis layer materializes as ΔT_m, signifying an increment of precisely 1.13 °C, and this phenomenon is uniquely associated with the 4 GHz MW frequency.

Moving to the dermis layer, the estimated T_m at $t = 180$ s are 38.23 °C for 0.9 GHz, 38.29 °C for 1.8 GHz, 37.95 °C for 2.45 GHz, and 38.57 °C for 4 GHz. The maximum temperature increase in the dermis for the 4 GHz frequency is $\Delta T_m = 0.34$ °C.

In the subcutaneous skin layer, the maximum mean temperature (T_m) observed at t = 180 s are 37.95 °C for 0.9 GHz, 38.99 °C for 1.8 GHz, 37.83 °C for 2.45 GHz, and 38.35 °C for 4 GHz.

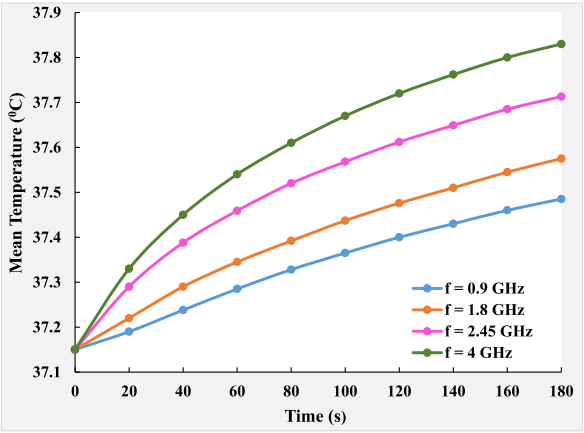

Fig. 9. Mean temperature (T_m) of the total computational domain for MW frequencies (i) 0.9 GHz, (ii) 1.8 GHz, (iii) 2.45 GHz, and (iv) 4 GHz, with $P = 12$ W, $\tau = 20$ s.

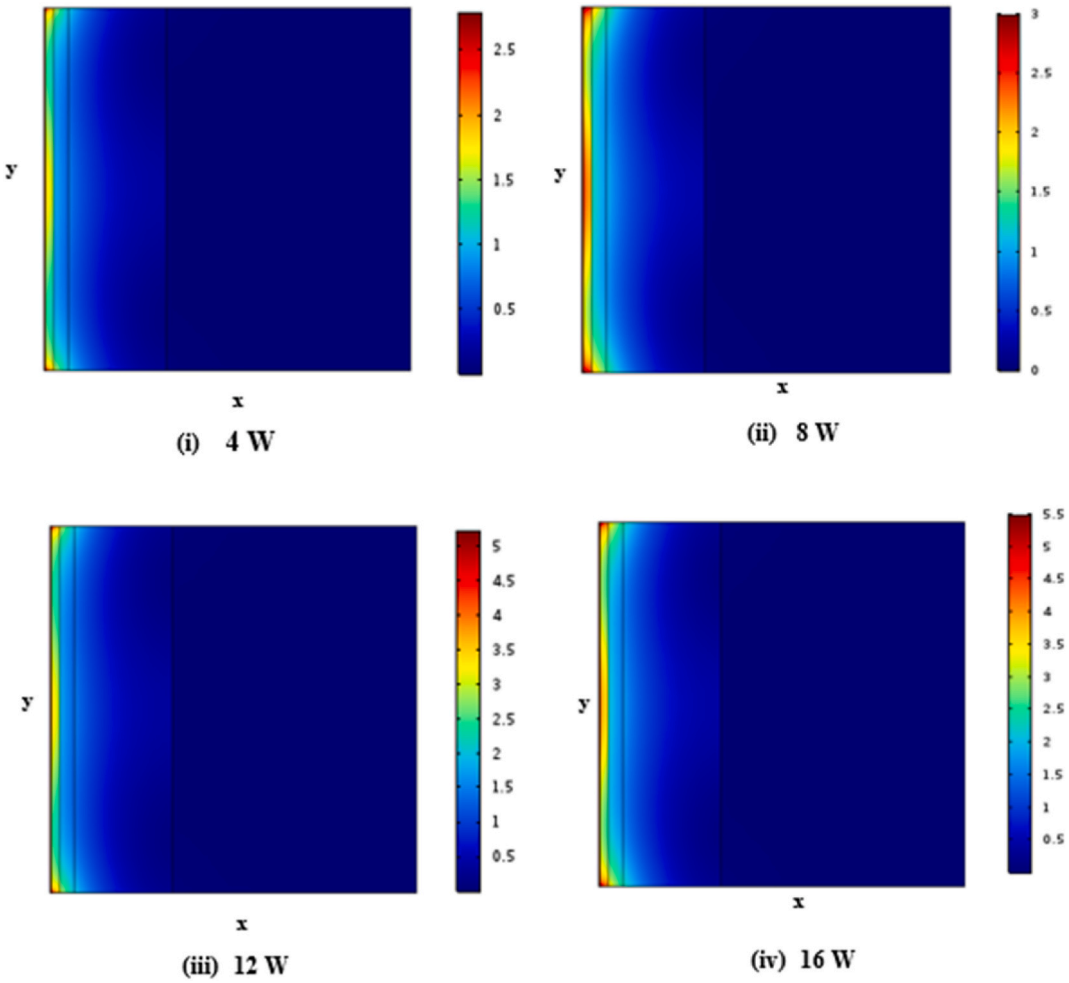

Fig. 10. Effect of MW power input (P) (i) 4 W, (ii) 8 W, (iii) 12 W, and (iv) 16 W, on MW power dissipation density (W/m^3) absorbed by skin tissue with $f = 2.45$ GHz, $\tau = 20$ s, and $t = 50$ s.

For the inner tissue layer, the estimated T_m at $t = 180$ s are 37.43 °C for 0.9 GHz, 37.79 °C for 1.8 GHz, 37.68 °C for 2.45 GHz, and 37.72 °C for 4 GHz. The temperature increase for the 4 GHz frequency is $\Delta T_m = 0.29$ °C.

Remarkably, it is worth mentioning that the acme mean temperature attainable under the influence of a 4 GHz MW frequency culminates at precisely 39.52 °C, featuring a discernible mean temperature elevation of ΔT_m, quantified as 1.8 °C. Although the heated area is primarily within the epidermis layer for 4 GHz, the T_m spike is short-lived. Therefore, it is a reasonable deduction drawn from these outcomes that the incremental mean temperature elevation, by its subtle nature, cannot impart any significant thermal detriment to the integrity of the examined tissues.

Within the confines of Fig. 8, we offer a comprehensive exposition that delves into the comparative thermal effects induced by diverse microwave frequencies through the prism of SAR methodologies, meticulously assessed on a horizontal cross-sectional slice of human dermal tissue at a designated heating duration of $t = 180$ s, originating from a radiation source characterized by plane wave properties. Determining the data extraction line or arc length is precisely situated at the central point of the superficial layer's longitudinal extent. The culmination of these SAR values attains a remarkable magnitude, attesting to SAR = 221 W per kilogram for the 0.9 GHz frequency, SAR = 319 W per kilogram for the 1.8 GHz frequency, SAR = 358 W per kilogram for the 2.45 GHz frequency, and SAR = 384 W per kilogram for the 4 GHz frequency. It is glaringly evident that the intricate SAR distribution pattern within the fabric of human skin is profoundly molded and influenced by a symbiotic interplay between the frequency of electromagnetic exposure and the intricate dielectric properties inherently residing within the bodily tissue. Furthermore, SAR values decrease rapidly as they penetrate deeper into the skin.

Fig. 9 shows the mean temperature (T_m) within the four-layered skin (total computational domain), calculated using equation (13) for various exposure durations and MW frequencies, denoted as $f = 0.9$, 1.8, 2.45, and 4 GHz. Temperature near the exposure source is notably elevated, marking a noteworthy thermal occurrence. The apogee of thermal manifestation is discerned within the epidermis layer, where the highest attainable temperatures materialize. In particular, when scrutinizing the specific microwave frequency of $f =$ 0.9 GHz, the estimated maximal mean temperature generated by the MW power registers at 37.49 °C, progressively escalating to 37.58 °C for $f = 1.8$ GHz, further advancing to 37.71 °C or $f = 2.45$ GHz, and ultimately culminating at 37.83 °C for $f = 4$ GHz, all within the confines of the temporal frame marked at $t = 180$ s.

From this figure, it is noticed that at the initial stage (from 0 to 180 s), there are dramatic changes in the mean temperature values of the different layers of skin for all frequency variations. After 180 s, the temperature values change slightly and become almost steady. This observation emphasizes that T_m increases with prolonged exposure durations and higher microwave frequencies.

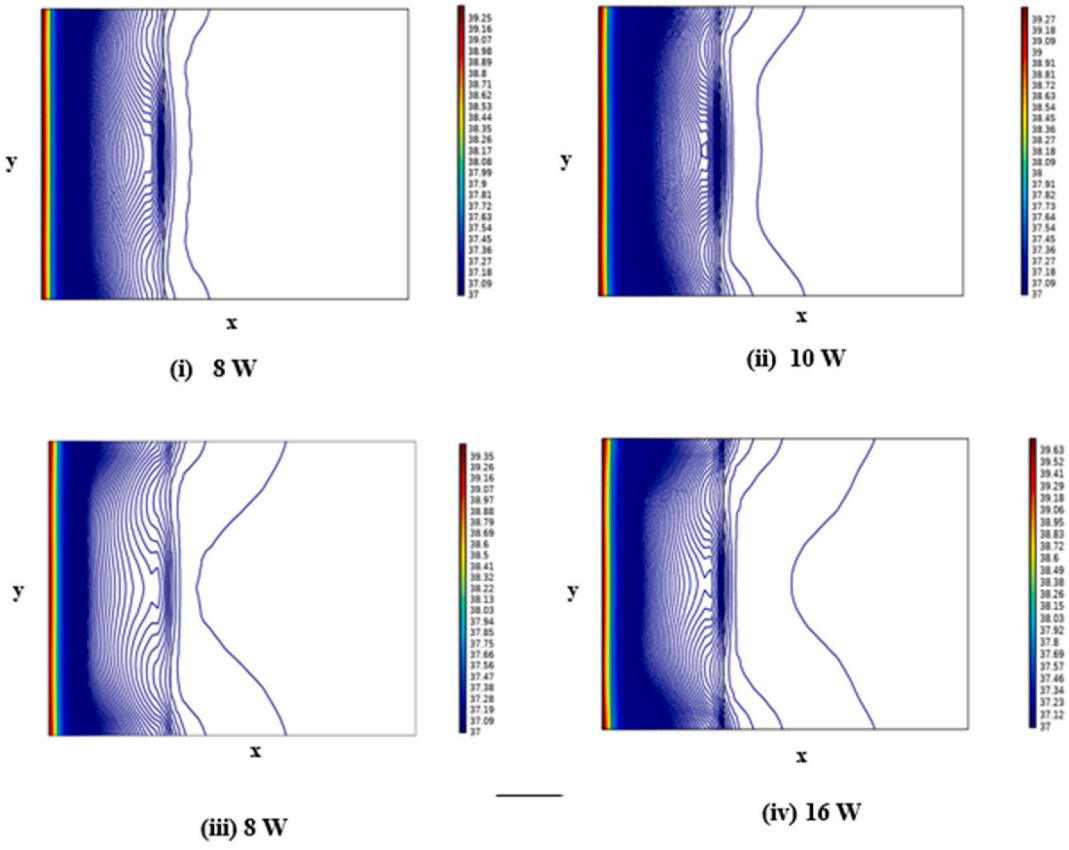

Fig. 11. Effect of MW power input (P) (i) 4 W, (ii) 8 W, (iii) 12 W and (iv) 16 W, on isothermal lines with $f = 2.45$ GHz, $\tau = 20$ s, and $t = 50$ s.

5.2. Effect of MW power

Fig. 10 through 13 shed light on the influence of input power levels (ranging from $P = 4$–16 W) on microwave power dissipation within human skin tissue using TWMBT. In these analyses, we maintain specific parameters constant: microwave frequency (f) at 2.45 GHz and exposure duration (τ) at 20 s.

Fig. 10 (i-iv) is a visual manifestation illustrating the microwave power density's absorption by the tissue of the skin precisely at the time point t, which is equal to 50 s. This analysis considers four discrete input microwave power levels: $P = 4$, 8, 12, and 16 W. From the visualization, it becomes evident that the absorbed power density experiences a substantial increase near the exposure source and extends uniformly across the entirety of the dermal tissue for all four power levels. As input power (P) increases, the heated area within the tissue also expands. This suggests that higher input power leads to a broader heating effect, which, unfortunately, affects a more significant portion of the skin tissue.

Within Fig. 11 (i-iv), we gain valuable insights from the contour plot of isothermal lines that depict the distribution of thermal energy within biological tissue. Notably, the epidermis layer exhibits a focal point of maximum temperature, with $P = 16$ W generating the highest temperature. It's worth noting that while increasing microwave power does lead to temperature elevation, the change remains relatively modest. Consequently, there is a minimal risk of causing damage to healthy tissue. The temperature escalation initially follows a linear trajectory; however, upon surpassing a specific threshold, additional influential factors such as diffusion and the thermal conduction caused by blood perfusion become significant contributors, culminating in the emergence of a saturation regime.

Fig. 12 (i-iv) provides an animated depiction that encapsulates the temporal evolution of mean temperature (T_m) variations across the distinct layers of the skin, encompassing the epidermis, dermis, subcutaneous layer, and deeper inner tissue regions. This evolution is observed under the influence of varying input power levels. In the epidermis layer, we observe maximum T_m of 39.01 °C for $P = 4$ W, 39.19 °C for $P = 8$ W, 39.31 °C for $P = 12$ W, and 39.58 °C for $P = 16$ W at t = 180 s. Similarly, maximum T_m in the dermis, subcutaneous, and inner tissue layers increase with higher input power levels, showing a similar trend. As the input power (P) increases, the heated area within the skin tissue expands, emphasizing the need for careful consideration when applying microwave energy to minimize potential effects on healthy tissue.

Fig. 13 provides a comprehensive analysis detailing the mean temperature existing within the tissue of the human skin (total computational domain) using equation (13) under different exposure durations for four specific input power levels, denoted as $P = 4$ W, $P = 8$ W, $P = 12$ W, and $P = 16$ W. It's evident that temperatures near the exposure source are significantly elevated, and the epidermis layer consistently registers the highest temperatures.

Specifically, Fig. 13 represents the mean temperature (T_m) of the total computational domain, measured using equation (12), where the changes against time duration from 0 to 180 s are apparent. The maximum temperature recorded for $P = 4$ W is 37.87 °C, which

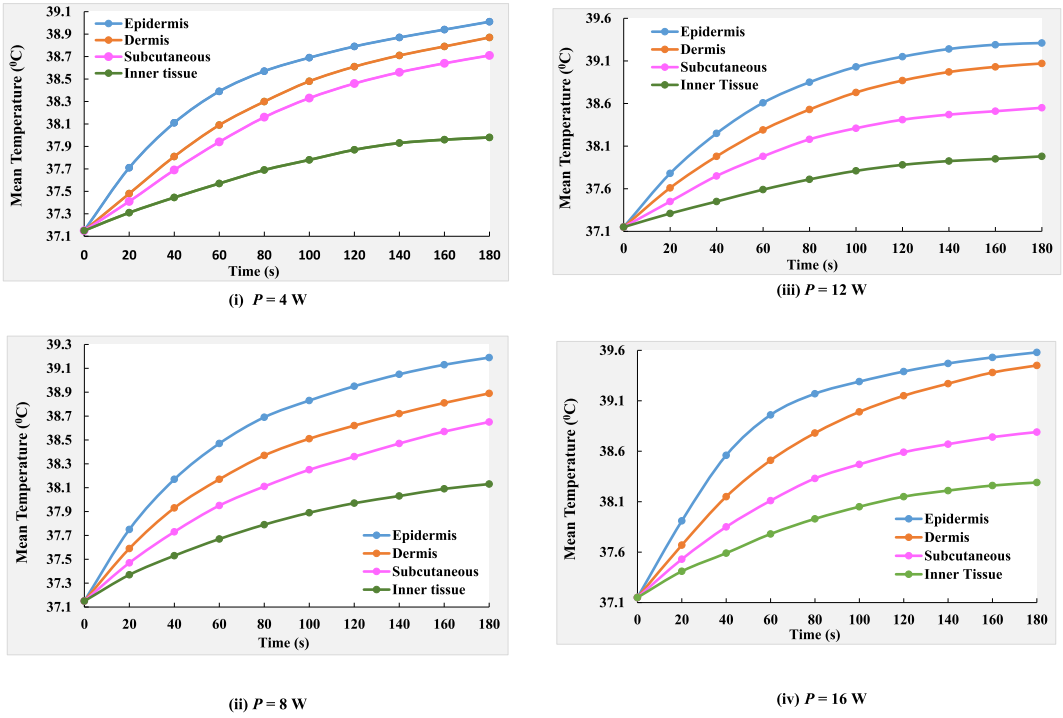

Fig. 12. Impact of input power (P) (i) 4 W, (ii) 8 W, (iii) 12 W, and (iv) 16 W on mean temperature (T_m) of different layers at different times with $f = 2.45$ GHz, and $\tau = 20$ s.

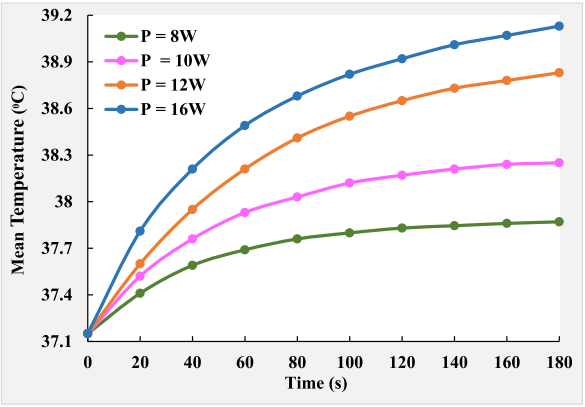

Fig. 13. Mean temperature (T_m) of total computational domain against $t = 0$–180 s, and for different microwave input power with $f = 2.45$ GHz and $\tau = 20$ s.

slightly increases to 38.25 °C for $P = 8$ W, 38.83 °C for $P = 12$ W, and 39.13 °C for $P = 16$ W. These observations underscore that both time and input MW power contribute to temperature elevation. Notably, we observe a rapid T_m increase when the MW power is set at $P = 16$ W. Consequently, the risk of causing harm to healthy skin tissue remains exceedingly low. This figure shows that for all MW input variations, there are significant changes in the mean temperature values of the four-layered skin tissue during the phase (Fig. 13). The T_m measurements fluctuate slightly and then nearly stabilize during the phase after 180 s. In summary, the findings suggest that precise control over exposure time and input power levels can be crucial in minimizing any potential adverse effects on healthy skin tissue during MW applications.

Fig. 14 presents a graphical representation of the contour plot of the temperature surface of tissue layers. This visual rendering elucidates the spatial allocation of temperature within the four-layered dermal tissue (epidermis, dermis, hypodermis, subjacent cells) at a specific point in time, namely, $t = 50$ s. These visual insights are derived from experiments conducted under controlled conditions featuring a consistent microwave input power of $P = 12$ W and a fixed frequency of $f = 2.45$ GHz. This representation reveals that microwave energy absorption by the skin tissue leads to elevated temperatures. The highest temperature of this contour plot is recorded at the exposure site, measuring approximately 39.9 °C. As we move away from this central point, the temperature gradually decreases, settling at about 37 °C near the outer limits of the computational domain. It becomes manifestly apparent that a lower temperature blood perfusion exerts a discernible influence in constraining the propagation of the thermally heated region. The temperature increased by approximately 2.90 °C. A combination of material properties can explain this rise, the efficiency of MW heating, and numerical truncation errors. The MW power levels, the application frequency, and the exposure duration significantly influence the temperature increase. Additionally, some research [4,7,11,30] has found a low-temperature enhancement, indicating that the observed temperature rise in the present result is evident.

5.3. Comparison between Pennes' BHE and TWMBT

5.3.1. Due to relaxation time

Figs. 15 and 16 display the mean temperature (T_m) variations within the skin layers (including epidermis, dermis, subcutaneous tissues, and inner tissues) during a 180-s exposure. Exploring these variances encompasses an assessment spanning an array of relaxation time (τ) values, specifically τ durations of 0, 10, 20, 30, and 40 s. The investigation in question meticulously delves into a multifaceted array of scenarios. These encompass a comprehensive assessment of diverse microwave frequencies, namely, 0.9 GHz, 1.8 GHz, 2.45 GHz, and 4 GHz, all sustained at a steadfast power (P) level of 12 W. Furthermore, it intricately scrutinizes various input power magnitudes, spanning 4 W, 8 W, 12 W, and 16 W. At the same time, the microwave frequency remains unwavering at 2.45 GHz, and the relaxation time (τ) is held constant at 20 s.

A noteworthy observation emerges as we analyze the mean temperature profiles derived from Pennes' BHE and TWMBT (with τ set to 0 s) in all the scenarios. It becomes evident that these T_m profiles remain identical in all cases. This uniformity strongly suggests that when τ is effectively reduced to zero seconds, Pennes' BHE and TWMBT converge, indicating that Pennes' BHE can be regarded as a specific instance or a particular case within the broader framework of TWMBT.

Within the dynamic phase, Pennes' BHE predicts the zenith of mean temperature, concurring with the temperature attributed to TWMBT with τ established at 0 s. On the converse, as relaxation times (τ) are augmented, the prognosis tends toward lower T_m levels, with the nadir of the temperature spectrum being ascribed to TWMBT when τ is specified as 40 s. These meticulous observations are delineated in Figs. 15 and 16.

Figs. 15 and 16 confirm that mean temperature increases at a swifter pace when using shorter relaxation times, in contrast to the T_m trends associated with longer relaxation times. A higher thermal relaxation time signifies a more robust thermal wave, wherein heat propagates primarily in waveform with minimal diffusion.

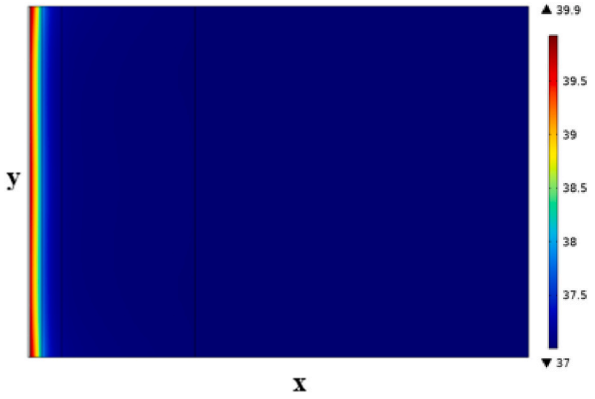

Fig. 14. Contour plot of temperature surface of four-layered human skin at $P = 12$ W, $f = 2.45$ GHz, and $t = 50$ s.

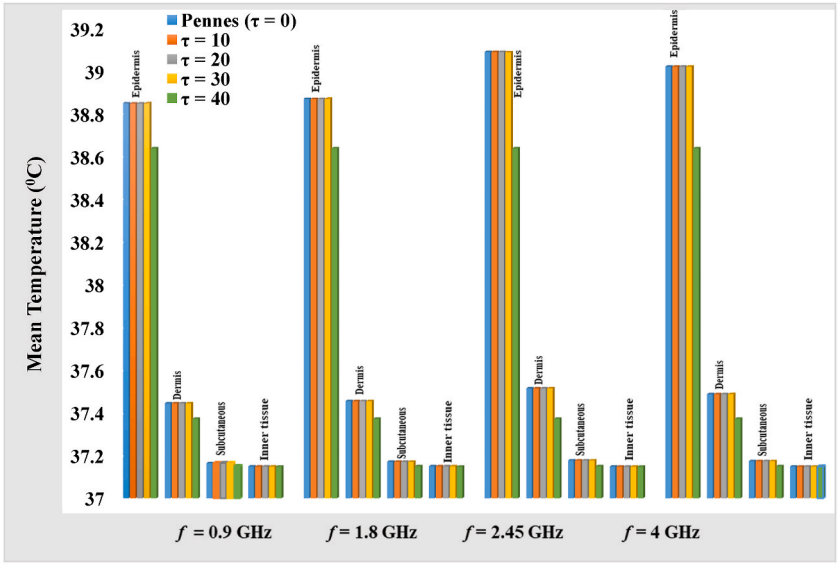

Fig. 15. Mean temperature (T_m) of different layers for relaxation times against frequency with $P = 12$ W, $t = 180$ s.

5.3.2. Due to temperature increment (present result and Ozen et al. [1])

A comparative analysis of temperature increment (in °C) over different time intervals (in seconds) and contrasted our findings with those presented by (Ozen et al. [1]). Fig. 17 showcases this comparison, focusing on a frequency of 2.45 GHz and a heat flux of $q = 63.1$ W/cm^2. Their research (Ozen et al. [1]) investigated temperature oscillations within the dermal layer at a depth measuring 1.2 mm beneath the skin's surface. For this comparison, the parameters are characterized by ω_b set at 0.5, the thermal conductivity denoted by k at 0.2 W per meter per degree Celsius, and a time constant represented as τ with a value of 20 s. The purple and red colours represent the results of temperature increment versus time using Pennes' BHE and TWMBT, respectively. These defined parameters are concurrently applied while subjecting the system to MW radiation at power densities of 63.1 mW per square centimeter, occurring at a specific frequency of 2.45 GHz.

Our analysis reveals that more considerable relaxation time (τ) values correspond to lower temperature predictions. Consequently, TWMBT consistently yields lower temperature curves compared to Pennes' equation. When the exposure period is relatively brief, the curve's characteristics are predominantly influenced by the source term, leading to a linear temperature rise. It's important to emphasize that the difference in accuracy between the two investigations is minimal. Within this comparative assessment, we observe a high degree of agreement between our present study (indicated by dot lines) and the results reported by (Ozen et al. [1]) (solid lines). This alignment in findings underscores the robustness and accuracy of the TWMBT model in predicting temperature variations in response to microwave exposure. The graph depicts the evolution of heat increase over time. It reveals that initially, TWMBT forecasts a lower heat rise than Pennes' equation. Nevertheless, as the exposure time progresses toward a steady state, TWMBT's predictions converge with Pennes' equations.

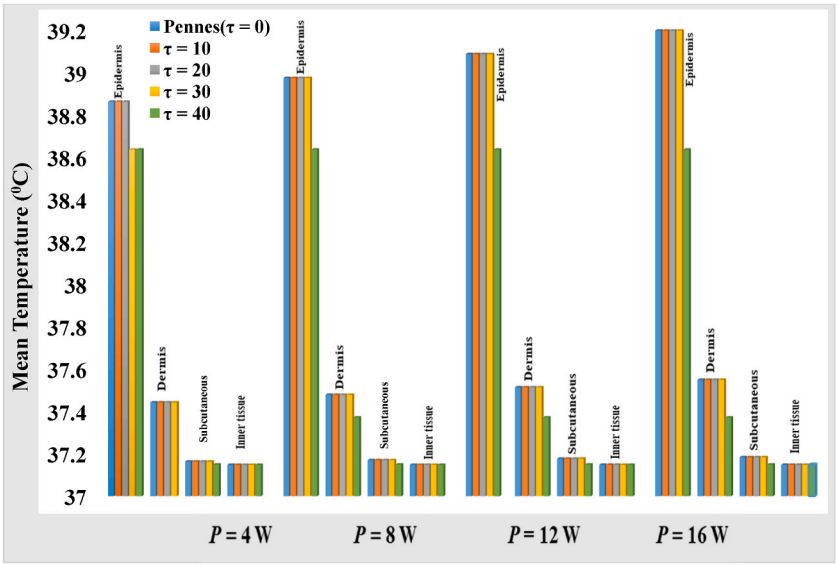

Fig. 16. Mean temperature (T_m) of several layers under varying relaxation times against input power with $f = 2.45$ GHz, $t = 180$ s.

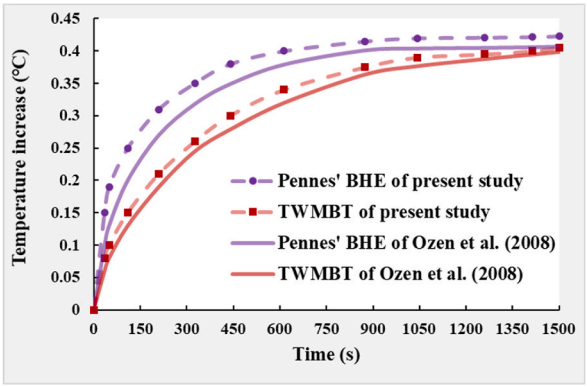

Fig. 17. Comparison of temperature increment from the present result (dot line) and (Ozen et al. [1]) (solid line).

6. Conclusions

This research represents a comprehensive numerical investigation into the intricate interplay of bioheat transfer and electromagnetic wave propagation within skin tissue subjected to microwave frequencies over 180 s. The study encompasses various microwave frequencies, input power levels, and relaxation times. To derive a numerical solution, we must grapple with the governing equations about the intricate realms of bioheat transfer and the propagation of EM waves. This is accomplished through the application of the FEM, employing the Galerkin method of weighted residuals.

Noteworthy findings and conclusions have emerged from this investigation.

- Comparative analysis between the conventional Pennes' bioheat and TWMBT reveals that they yield identical heat distribution patterns in steady-state conditions.
- Within the epidermis layer, temperatures ranging from approximately 38.98 °C are observed for frequency variation.
- At a microwave frequency of 0.9 GHz, the skin encounters the highest total power dissipation density (W/m^3), while the lowest is at 4 GHz.
- When it comes to power input, the maximum total power dissipation density (W/m^3) occurs at 16 W, whereas the lowest density is predicted at 4 W.
- At a frequency of 4 GHz, the SAR experiences its zenith, denoting the point at which it quantifies the most substantial extent of EM energy absorption by skin tissue. Conversely, at 0.9 GHz, the SAR descends, signifying its minimum quantification of EM energy absorption by the same tissue.

- The study highlights that a higher thermal relaxation time amplifies the thermal wave's dominance, leading to heat propagation predominantly in waveform with minimal diffusion.
- The research additionally elucidates that the influence exerted by relaxation times on temperature fluctuations becomes appreciable solely under circumstances characterized by brief exposure durations.
- Integrating a thermal relaxation time into a thermal wave model, like in the case of TWMBT, yields enhanced temperature predictions when contrasted with the conventional Pennes' bioheat equation.

To summarize, this study yields valuable insights into the complex dynamics of energy absorption within human skin tissue exposed to microwave radiation. It underscores the importance of considering various parameters in assessing the thermal impact and demonstrates the utility of the TWMBT model in predicting temperature distributions with enhanced accuracy. These insights may have implications for the advancement of clinical thermal technologies and applications within the field of thermal medicine, including areas such as lasers and cancer hyperthermia.

CRediT authorship contribution statement

Zerin Jahan Tasnim: Writing – original draft, Validation, Methodology, Investigation, Formal analysis. **R. Nasrin:** Writing – review & editing, Supervision, Software, Methodology, Conceptualization.

Data availability

No data is used for the research described in the article.

Declaration of competing interest

The authors declare that they have no known competing financial interests or personal relationships that could have appeared to influence the work reported in this paper.

References

[1] S. Ozen, S. Helhel, O. Cerezci, Heat analysis of biological tissue exposed to microwave by using thermal wave model of bioheat transfer (TWMBT), Burns 34 (2008) 45–49.
[2] International Commission on Non-ionizing Radiation Protection (ICNIRP), Guidelines for limiting exposure to electromagnetic fields (100 KHz to 300 GHz), Health Phys. 118 (2020) 483–524.
[3] D.L. Means, K.W. Chan, Evaluating compliance with FCC guidelines for human exposure to radiofrequency electromagnetic fields, Federal Communications Commission Office of Engineering and Technology 65 (2001) 1–57.
[4] IEEE, IEEE standard for safety levels concerning human exposure to electric, magnetic, and electromagnetic fields, 0 Hz to 300 GHz, EEE Standard C95.1–2019 (2019).
[5] O. Bejenaru, C. Lazarescu, S. Vornicu, V. David, Specific absorption rate evaluation in case of exposure of the human body to radiofrequency electromagnetic field generated by mobile communications. International Conference and Exposition on Electrical and Power Engineering, EPE), 2008, pp. 1004–1009.
[6] J.F. Bakker, M.M. Paulides, E. Neufeld, A. Christ, N. Kuster, G.Cv Rhoon, Children and adults exposed to electromagnetic fields at the ICNIRP reference levels: theoretical assessment of the induced peak temperature increase, Phys. Med. Biol. 56 (2011) 4967.
[7] J. Kaur, Numerical analysis of heat transfer in multilayered skin tissue exposed to 5g mobile communication frequencies, J. Therm. Eng. 7 (2021) 103–116.
[8] A. Peyman, C. Gabriel, E.H. Grant, G. Vermeeren, L. Martens, Variation of the dielectric properties of tissues with age: the effect on the values of SAR in children when exposed to walkie-talkie devices, Phys. Med. Biol. 54 (2009) 227–241.
[9] T. Wessapan, S. Srisawatdhisukul, P. Rattanadecho, Numerical analysis of specific absorption rate and heat transfer in the human body exposed to leakage electromagnetic field at 915 MHz and 2450 MHz, J. Heat Tran. 133 (2011) 051101.
[10] M. Kojima, Y. Suzuki, K. Sasaki, M. Taki, K. Wake, S. Watanabe, M. Mizuno, T. Tasaki, H. Sasaki, Ocular effects of exposure to 40, 75, and 95 GHz millimeter waves, J. Infrared, Millim. Terahertz Waves 39 (2018) 912–925.
[11] D.A. Stewart, T.R. Gowrishankar, J.C. Weaver, Skin heating and injury by prolonged millimeter-wave exposure: a theory based on a skin model coupled to a whole-body model and local biochemical release from cells at supraphysiologic temperatures, IEEE Trans. Plasma Sci. 34 (2006) 1480–1493.
[12] A.M.M. Mukaddes, R. Shioya, M. Ogino, D. Roy, R. Jaher, Finite element-based analysis of bioheat transfer in human skin burns and afterward, Int. J. Comput. Methods 18 (2021) 2041010.
[13] J.C. Lin, Z. Wang, Hearing of microwave pulses by humans and animals: effects, mechanism, and thresholds, Health Phys. 92 (2007) 621–628.
[14] M.C. Ziskin, J. Morrissey, Thermal thresholds for teratogenicity, reproduction, and development, Int. J. Hyperther. 27 (2011) 374–387.
[15] X. Huang, P.K. Jain, I.H. El-Sayed, M.A. El-Sayed, Plasmatic photothermal therapy (PPTT) using gold nanoparticles, Laser Med. Sci. 23 (2008) 217–228.
[16] S. Lin, C. Li, Semi-analytical solution of bioheat conduction for multi-layer skin subjected to laser heating and fluid cooling, J. Mech. Med. Biol. 17 (2017) 175–229.
[17] R. Amare, E. Hodneland, J.A. Roberts, A.A. Bahadori, S. Eckels, Modeling a 3-D multiscale blood-flow and heat-transfer framework for realistic vascular systems, Sci. Rep. 12 (2022) 14610.
[18] D.B. Gurung, D.C. Shrestha, Mathematical study of temperature distribution in human dermal part during physical exercise, J. Inst. Eng. 12 (2016) 63–76.
[19] J. Dutta, B. Kundu, Hybrid analytical models to estimate non-equilibrium temperatures in live-tissues based on appropriate initial thermal-field and non-invasive therapeutic heating, J. Appl. Phys. 129 (10) (2021).
[20] P. Keangin, T. Wessapan, P. Rattanadecho, Analysis of heat transfer in deformed liver cancer modeling treated using a microwave coaxial antenna, Appl. Therm. Eng. 31 (2011) 3243–3254.
[21] J. Dutta, B. Kundu, S.J. Yook, Three-dimensional thermal assessment in cancerous tumors based on local thermal non-equilibrium approach for hyperthermia treatment, Int. J. Therm. Sci. 159 (2021) 106591.
[22] P. Rattanadecho, P. Keangin, Numerical study of heat transfer and blood flow in two-layered porous liver tissue during microwave ablation process using single and double slot antenna, Int. J. Heat Mass Tran. 58 (2013) 457–470.
[23] C. Biswas, R. Nasrin, M.S. Ahmad, Numerical analogy of bioheat transfer and microwave cancer therapy for liver tissue, Heat Transfer 51 (2022) 6403–6430.
[24] M. Tung, M. Trujillo, J.A.L. Molina, M.J. Rivera, E.J. Berjano, Modeling the heating of biological tissue based on the hyperbolic heat transfer equation, Math. Comput. Model. 50 (2008) 665–672.

[25] R. Fazlali, H. Ahmadikia, Analytical solution of thermal wave models on skin tissue under arbitrary periodic boundary conditions, Int. J. Thermophys. 34 (2013) 139–159.
[26] J. Dutta, B. Kundu, Two-dimensional closed-form model for temperature in living tissues for hyperthermia treatments, J. Therm. Biol. 71 (2018) 41–51.
[27] M. Marin, A. Hobiny, I. Abbas, Finite element analysis of nonlinear bioheat model in skin tissue due to external thermal sources, Mathematics 9 (2021) 1459.
[28] F. Xu, T. Lu, K.A. Seffen, Dual-phase-lag model of skin bioheat transfer. Proceedings of the 2008 International Conference on Bio-Medical Engineering and Informatics, Sanya, China, 2008, pp. 505–511.
[29] W. Kaminski, Hyperbolic heat conduction equation for material with a nonhomogeneous inner structure, ASME Journal of Heat Transfer 112 (1990) 555–560.
[30] K. Mitra, S. Kumar, A. Vedavarz, M.K. Moallerni, Experimental evidence of hyperbolic heat conduction in processed meat, ASME Journal of Heat Transfer 117 (1995) 568–573.
[31] K.C. Liu, Y.N. Wang, Y.S. Chen, Investigation on the bioheat transfer with the dual-phase-lag effect, Int. J. Therm. Sci. 58 (2012) 29–35.
[32] J. Dutta, B. Kundu, Two-dimensional hybrid analytical approach for the investigation of thermal aspects in human tissue undergoing regional hyperthermia therapy, Proc. IME C J. Mech. Eng. Sci. 234 (2020) 3951–3966.
[33] B. Kundu, Exact analysis for propagation of heat in a biological tissue subject to different surface conditions for therapeutic applications, Appl. Math. Comput. 285 (2016) 204–216.
[34] J. Kaur, S.A. Khan, Influence of relaxation times on heat transfer in human head exposed to microwave frequencies, J. Therm. Eng. 7 (4) (2021) 934–950.
[35] P. Antaki, New interpretation of non-Fourier heat conduction in processed meat, J. Heat Tran. 127 (2005) 189–193.
[36] A. Banerjee, A. Ogale, C. Das, K. Mitra, C. Subramanian, Temperature distribution in different materials due to short pulse laser irradiation, Heat Tran. Eng. 26 (2005) 41–49.
[37] A. Hobiny, I.A. Abbas, Nonlinear analysis of dual-phase lag bio-heat model in living tissues induced by laser irradiation, J. Therm. Stresses 43 (2020) 503–511.
[38] B. Kundu, D. Dewanjee, A new method for non-Fourier thermal response in a single layer skin tissue, Case Stud. Therm. Eng. 5 (2015) 79–88.
[39] J. Dutta, B. Kundu, A revised approach for an exact analytical solution for thermal response in biological tissues significant in therapeutic treatments, J. Therm. Biol. 66 (2017) 33–48.
[40] T. Saeed, I. Abbas, Finite element analyses of nonlinear DPL bioheat model in spherical tissues using experimental data, J Mechanics Based Design of Structures and Machines 50 (2020) 1287–1297, https://doi.org/10.1080/15397734.2020.1749068.
[41] X.Z. Liu, Y. Zhu, F. Zhang, X.F. Gong, Estimation of temperature elevation generated by ultrasonic irradiation in biological tissues using the thermal wave method, Chin. Phys. 22 (2013) 1–43.
[42] R. Essam, A. Elsaid, W.K. Zahra, Bioheat transfer in skin tissue using fractional Weinbaum-Jiji model, in: 2023 International Conference on Fractional Differentiation and its Applications (ICFDA), 2023, pp. 1–5.
[43] R. Nasrin, S.A. Sawmpa, Hepatic tumor ablation using electric current and bioheat transfer model: a 3D numerical analysis, J. Nav. Architect. Mar. Eng. 21 (1) (2024) 53–66, https://doi.org/10.3329/jname.v21i1.61347.
[44] R. Nasrin, A. Hossain, I. Zahan, Blood flow analysis inside a stenotic artery using power-law fluid model, Research and Development in Material Science 13 (2020) 1360–1368, https://doi.org/10.31031/RDMS.2020.13.000803.
[45] H.H. Pennes, Analysis of tissue and arterial blood temperatures in the resting human forearm, J. Appl. Physiol. 1 (1998) 93–122.
[46] Shih, T.C., Yuan, P., Lin, W.L., Kou, H.S., Analytical analysis of the Penne's bioheat transfer equation with sinusoidal heat flux condition on skin surface. Med. Eng. Phys. 29, 946-953.
[47] C. Taylor, P. Hood, A numerical solution of the Navier-Stokes equations using finite element technique, Computer and Fluids 1 (1973) 73–89.
[48] D. Torvi, J. Dale, A finite element model of skin subjected to a flash fire, J. Biomech. Eng. 116 (1994) 250–255.